Preprint
UCRL-JC-138941

Warm, Dense Plasma Characterization by X-ray Thomson Scattering

O. L. Landen, S. H. Glenzer, R. C. Cauble, R. W. Lee, J. E. Edwards, and J. S. Degroot

This article was submitted to
XXVI European Conference on Laser Interaction on Matter
Praha, Czech Republic
June 12-16, 2000

July 18, 2000

U.S. Department of Energy
Lawrence
Livermore
National
Laboratory

Warm, Dense Plasma Characterization by X-ray Thomson Scattering

Otto L. Landen, S.H. Glenzer, R.C. Cauble, R.W. Lee, J.E. Edwards, and J.S. Degroot*

Lawrence Livermore National Laboratory, Livermore CA 94551
*U.C. Davis, Davis, CA 95616

ABSTRACT

We describe how the powerful technique of spectrally resolved Thomson scattering can be extended to the x-ray regime, for direct measurements of the ionization state, density, temperature, and the microscopic behavior of dense cool plasmas. Such a direct measurement of microscopic parameters of solid density plasmas could eventually be used to properly interpret laboratory measurements of material properties such as thermal and electrical conductivity, EOS and opacity. In addition, x-ray Thomson scattering will provide new information on the characteristics of rarely and hitherto difficult to diagnose Fermi degenerate and strongly coupled plasmas.

Keywords: dense plasmas, x-rays, Thomson scattering, Compton scattering, strongly coupled plasmas

1. INTRODUCTION

The microscopic behavior of warm (3 - 30 eV), solid density matter for which the electrostatic potential energy between particles exceeds the thermal energy has been the subject of numerous theoretical studies[1-4] and no known definitive experiments. There has been a recent surge in interest in understanding solid density, strongly coupled plasma properties[5-8] partially motivated by the emergence of short-pulse high power lasers with the ability to heat solids before significant hydrodynamic motion occurs.[9] Current microscopic experimental techniques are limited. Optical probing only provides information on rarefied surface layers since solid density plasmas are overdense to visible and UV light. Absorption spectroscopy can only probe near high energy ionization edges since the open line transitions are at energies of tens of eV, too soft a photon energy to allow sufficient probe transmission for reasonably-sized plasmas.

We propose a powerful, alternative diagnosis method, spectrally-resolved multi-keV x-ray scattering. By spectrally discriminating between the coherent (Rayleigh), Compton and Thomson scattering components, we expect to gather information on many microscopic parameters, including the free and bound electron densities and fractions, temperature, plasma flow velocity if any, and plasma collisionality. The Omega facility at the Laboratory for Laser Energetics can provide the required photon flux for single-shot detection and the required uniform heating by virtue of its many beams covering a full sphere.

We will prepare a uniformly heated (up to 30 eV) solid density mm-scale Be plasma by volumetric preheating using multi-keV x-rays from laser plasmas created at the Omega laser facility. Another multi-keV line radiator (at wavelength λ) produced from a second delayed laser plasma will provide the narrow ($\Delta\lambda/\lambda < .003$) line required for near backscatter x-ray Thomson scattering before the Be plasma cools or disassembles. The scattered photons will be collected and spectrally dispersed by a Von Hamos geometry Bragg crystal coupled to a gated framing camera. We expect to be able to determine both the Fermi energy (and hence free electron density) and electron temperature from the high frequency component of the Thomson scattered spectrum. We expect this first attempt at extending the versatility of laser Thomson scattering[10-12] to the x-ray regime to open the door for detailed strongly coupled plasma studies of great interest to the high energy density and plasma physics communities.

2. MOTIVATION

Fermi degenerate ($T_e < T_F$) and strongly coupled plasmas are present in a variety of laboratory[13-18] and astrophysical environments.[19-21] Thelatter plasmas can be characterized by the ratio Γ_{ee} of the Coulomb potential energy between free electrons to the kinetic energy of the free electrons being > 1. These are basic states of matter occurring at some location during the interaction between intense lasers and a solid. These are also regimes accesssed by the DT fuel during an ICF implosion, as shown on Fig. 1.

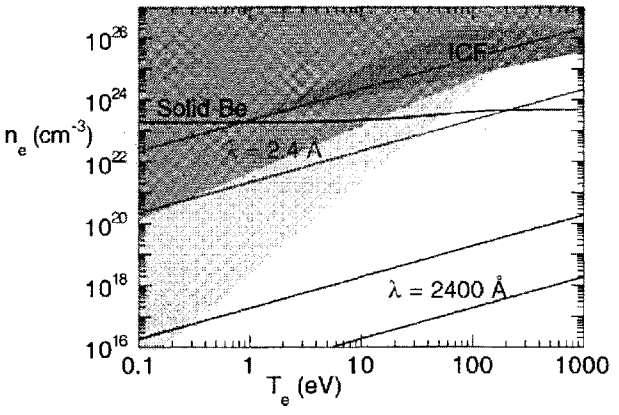

Figure 1: Electron density and temperature parameter space showing Fermi degenerate (upper left shaded) and strongly coupled plasma regimes (middle shaded), where lower edge of each regime set by $T_e = T_F$ and $\Gamma_{ee} = 1$, respectively. Line around $2x10^{23}$ cm^{-3} is solid Be equilibrium electron density (conduction and free electrons).[22] Solid sloped lines bound α =1-0.1, $\theta = 180°$ Thomson scattering regimes accessible for λ = 2400 and 2.4 Å probes. Upper right shaded region is ICF DT fuel regime during compression.

In Figure 1, the strongly coupled plasma and Fermi degenerate regimes are shown shaded in electron density n_e - electron temperature T_e space. For a given density at lower temperatures, the plasmas are either Fermi degenerate or only partially ionized, and hence in a sense only weakly coupled. At higher temperatures, they behave as ideal gases with insignificant inter-particle coupling. In between, the ideal gas approximation for plasma behavior breaks down. The concept of a Debye screening length breaks down since the Debye length λ_D becomes less than the average interparticle spacing. Various statistical mechanics models[23-25] differ by factors of several in the predicted electron-ion collisionality in this regime (see Fig. 2). Material properties such as electrical[26-29] and thermal conductivity,[6,30] opacity[31-33] and equation-of-state (EOS)[34,35] have been studied in this regime for resolving theoretical and calculational uncertainties. However, the usefulness of such measurements has been impaired because of the lack of an independent measurement of temperature and density.

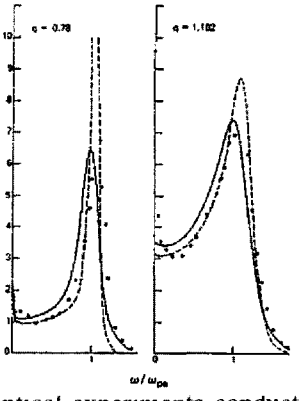

Figure 2: Predicted[25] collective scattering spectra (α = 3 and 2) for electron plasma wave resonances for strongly coupled dense plasma (Γ = 2, $n_e = 2x10^{24}$ cm^{-3}, T_e =14 eV). Dots, solid curve and dashed curve are predictions based on a Monte Carlo molecular dynamics code, a Fokker-Planck model and a Vlasov model incorporating a Hypernetted Chain model. The differences are principally related to differences in the calculated level of electron-ion collisional damping.

Moreover, the optical experiments conducted so far have either probed low density plasmas amenable to internal optical probing,[31,36,37] or attempted to infer conditions by probing overdense interfaces.[38] Figure 1 shows that to investigate deeply into the strongly coupled regime at the low densities amenable to optical probing, one must work at eV or sub-eV temperatures. This leads to either partial ionization and hence the complication of neighboring bound states and dominance of electron atom collisions, or the production of a transient over-ionized non-equilibrium state which will quickly recombine by three-body recombination. Surface probing of overdense plasmas is difficult to interpret[9,38-42] because density gradients as short as $\lambda/2\pi$ dramatically modify observables such as reflectivity and phase modulation.[39,43,44] Internal x-ray probing for strongly coupled plasmas at super-critical to super-solid density has relied so far on continuum edge spectroscopy and extended x-ray absorption fine-structure (EXAFS),[45-49] lineshape spectroscopy[16,50] or non-spectrally resolved x-ray scattering.[51-53] All rely on extensive modelling of both bound and free electron wave-functions, and densities to interpret the data, and the latter does not provide information on the ionization state or temperature of the material.

We propose to extend the power of spectrally resolved Thomson scattering to the x-ray regime, for direct measurements of the ionization state, density, temperature, and the microscopic behavior of strongly coupled plasmas. This would be the first direct measurement of microscopic parameters of solid density plasmas, which eventually could be used to properly interpret laboratory measurements of material properties such as thermal and electrical conductivity, EOS and opacity.

3. X-RAY THOMSON SCATTERING

Thomson scattering at a probe wavelength λ and angle θ is characterized by the scattering parameter α, proportional to the ratio of the probing scale-length $\lambda_s = \lambda/2\sin(\theta/2)$ to the Debye length: $\alpha = \lambda_s/2\pi\lambda_D$. For $\alpha < 1$, spectrally-resolved incoherent Thomson scattering provides information on the velocity v and hence temperature and directed flux of free electrons from the Doppler shifts experienced by scattered probe photons. For $\alpha > 1$, the collective scattering regime, the scattering is sensitive to temporal correlations between electron motion separated by more than a Debye length and hence the scattering is dominated by ion-acoustic and electron plasma wave resonances, the latter set by the well known Bohm-Gross dispersion relation. The frequency shift of the resonance is dependent on density through the plasma frequency while the width of the resonances yields information on the wave damping rates. In the intermediate regime near $\alpha = 1$, the form of the electron plasma high frequency component depends strongly on both the electron temperature and density, providing a robust internal measurement of these basic plasma parameters, confirmed by spectroscopy.[54]

Overplotted on Fig. 1 are the regimes accessible by Thomson scattering with $\alpha = 0.1$-1 and $\theta = 180°$ for various wavelength probes λ. Such Thomson scattering accesses regimes in which the Debye length is of order the probe wavelength (e.g. $\lambda_D \approx$ 1000 Å for a 2400 Å probe). By switching from a UV probe at 2400 Å to an x-ray probe at 2.4 Å, we can effectively probe plasmas with Debye lengths of the order of the interparticle spacing or shorter (1 Å). Stated differently, for a given plasma temperature, we should be able to access a density that is 6 orders of magnitude higher than previously attempted. In particular, Fig. 1 shows that the solid density regime (shown for beryllium as a dotted line) crosses the strongly coupled plasma regime precisely where it is accessible by 2.4 Å Thomson scattering.

For spectrally resolved x-ray Thomson scattering, one does not necessarily need an x-ray laser for the following reasons. First, since the experiment proposed here can provide valuable, new information on solid density plasmas by just resolving the high frequency Thomson scattered components, only probe linewidths $\Delta\lambda/\lambda$ of order v/c are required, = .003 at a few eV electron temperature. These can be provided by resonance lines from hot mid Z plasmas whose linewidths as determined by few keV ion motion and Stark broadening are less than the scattered Doppler widths as set by few eV electron motion (since the ion/electron mass is > 1000). Second, incoherent Thomson scattering ($\alpha < 1$) requires little or no probe transverse coherence, since the scattering from individual electrons for at least ideal plasmas is uncorrelated. In the collective scattering regime ($\alpha > 1$), scattering is sensitive to time-correlated electron motion between two positions separated by the probing scale length λ_s. For $\theta \approx 180°$, $\lambda_s \approx \lambda/2$, within the transverse coherence length of a totally incoherent source at a photon wavelength λ. Third, the fraction of scattered photons will be substantial. For example, for $n_e = 1.6\text{x}10^{23}$ cm^{-3}, a Thomson scattering cross-section of $\sigma = 6.6\text{x}10^{-25}$ cm^{-2}, and a pathlength x of 0.1 cm in low Z material, the fraction scattered = $n_e\sigma x$ = 0.01, close to the maximum desirable for avoiding multiple scatterings. Coupled with a realistic source solid angle of 0.1 steradians, the scattered fraction from an isotropic source is still 10^{-4}, orders of magnitude larger than the usual $10^{-(6\text{-}10)}$ fractions available for visible Thomson scattering at lower densities.

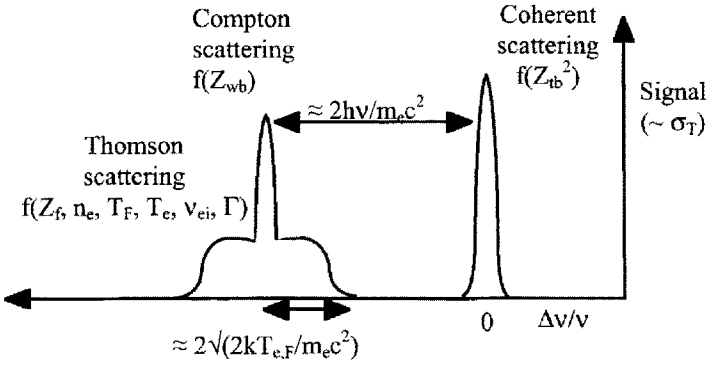

Figure 3: Schematic of spectrally-resolved x-ray backscattering spectrum expected, with information provided by each feature noted as f( ). The shape of the electron Thomson scattered feature will transition from a Fermi degenerate flattop distribution for $T_e << T_F$ to a Boltzmann distribution for $T_e >> T_F$. The peak labelled Compton scattering will be mixture of scattering from weakly bound electrons and low frequency ion acoustic-driven Thomson scattering from free electrons for values of $\alpha > 0.1$.

A schematic of the expected generic backscattered spectrum features is shown in Fig. 3. Coherent scattering[55] from tightly bound electrons (Z_{tb} of them per atom) should provide an unshifted peak at the probe wavelength whose intensity varies as Z_{tb}^2. Incoherent Compton scattering from weakly bound electrons[56-58] (Z_{wb} of them per atom) should provide a second peak downshifted in energy by $2h\nu/mc^2$, with an intensity varying as Z_{wb}. Thomson scattering from free electrons (Z_f of them per atom) should provide a dispersed spectrum centered on the Compton peak, with a spectrally integrated intensity varying as Z_f, and the form of the spectrum in general depending on the Fermi energy T_F, free electron density n_e, temperature T_e, electron-ion collisionality ν_{ei}, and strong coupling parameter Γ. Hence by spectrally resolving a scattered x-ray spectrum for the first time, we would gain access to an unparalleled source of information on warm dense matter.

For example, we should be able to infer Z_f, Z_{tb}, and Z_{wb} from the relative importance of coherent, incoherent and free electron scattering contributions. This would allow us to discriminate between different ionization balance models such as Thomas-Fermi and Inferno.[59] We should be able to infer the free electron temperature, Fermi energy T_F, hence electron density (and hence ionization state since the ion density is effectively hydrodynamically frozen) from the shape of the Thomson scattered spectrum for $\alpha < 1$. Furthermore, for strongly coupled plasmas, one of the more intriguing possibilities is the establishment of long-range coherence even in the plasma state.[60] In that case, one would need to increase the transverse coherence length of our incoherent source, easily accomplished by further distancing the source from the sample. If coherent plasma wave modes exist, then the Thomson scattering contribution should increase as the square of the number of coherent scatterers.

4. EXPERIMENTAL DESIGN

We have designed an x-ray scattering experiment optimized for the Omega laser facility capabilities which should provide high quality spectral data on a single shot. A detailed view of the target design is shown in Fig. 4. The emphasis here is to create a uniformly heated large-scale sample with known energy content that can be probed internally before it cools or disassembles appreciably. The previous published experiments alluded to have either been performed in the presence of large unknown density and temperature gradients, or unknown temperatures, requiring hydrodynamic modelling to constrain the interpretation of the data. The uniformity of heating is optimized here by using multi-keV x-rays over a narrow band (4-5 keV) to provide volumetric preheating, and by almost fully enveloping the sample by the pump source distributed over $\approx 3\pi$ steradians (see Fig. 4). The ratio of pump photon mean free path to sample size has been chosen to be large enough at 2x to provide a calculated, acceptable ±15% uniformity in the energy absorbed / sample atom at all positions inside the sample, yet small enough to provide adequate energy deposition.

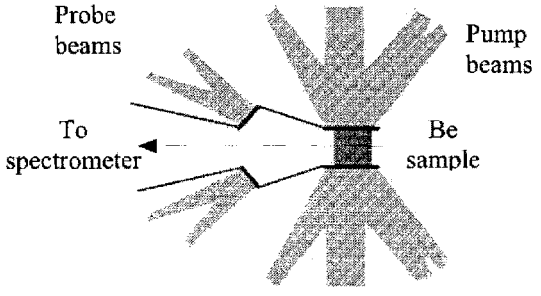

Fig. 4. Scaled schematic of proposed experimental set-up at Omega. Target is cylindrically symmetric about collection axis (dashed line). 20 kJ irradiates a thin CsI-coated plastic foil surrounding the central cylindrical Be sample, producing the 4-5 keV x-ray preheating source. A 5 keV Thomson scattering probe is produced on the left by irradiating a thin vanadium annular foil with 6 kJ of laser energy.

The percentage of the sample subject to shock compression and disassembly by rarefaction after preheating is minimized to the few % level by minimizing the surface area to volume of the sample (i.e. using a sample with similar dimensions in all three directions). The symmetric arrangement of beams at the Omega facility lend itself well to using a cylindrical sample overcoated on its curved surface with a thin high Z x-ray conversion layer transparent to its own multi-keV x-rays for providing the pump source (see Fig. 4). 42 of the 60 Omega beams can efficiently couple their energy onto this curved surface at incidence angles below 45°. 12 of the remaining beams can be used to provide a bright x-ray probe source using a mid Z x-ray conversion foil in the shape of an annulus. The complete target is cylindrically symmetric, making it amenable to direct two-dimensional (2D) modelling.

The detected signal is maximized by maximizing the number of potential scattering electrons, the probe solid angle subtended at the scatterer, and collection solid angle. The number of electrons heated to a given temperature for a given pump energy, photon energy and optimized sample geometry discussed above is maximized by maximizing the absorption mean free path (mfp) for the pump photons. This is achieved by using a low atomic number Z sample, and hence we propose using a Be sample as the lowest Z conveniently available solid. The scaling with atomic number Z is particularly strong since the cold mfp varies as $\approx Z^{3.5}$ well above ionization edges. Hence, the absorbed energy / atom for a given pump photon energy will scale as Z^{11} for a sample scaled in all dimensions by $1/Z^{3.5}$. For example, the ratio in absorbed energy / atom between Al (Z = 13), C (Z = 6) and Be (Z = 4) scaled experiments would then be $\approx 10^5:10^2:1$, but the number of potential free electron scatterers would be close to the inverse ratio of $10^5:10^2:1$. One could increase the pump mean free path by up to 10x and hence the number of scatterers in higher Z samples by 10^3 by doubling the pump photon energy (from 5 to 10 keV). However, this would be achieved the expense of greatly (> 10x) reduced conversion efficiency of laser to x-ray photons.[61]

The second advantage in using a low Z sample is the reduction in the bound electron scattering contribution ~ $(Z_{tb}^2 + Z_{wb})$ relative to the free electron contribution ~ Z_f. Hence, any bound electron scattering of the spectral wings of the probe source can be kept negligible compared to the dispersed free electron scattering contribution. For Be at ≈ 10 eV, we expect $Z_{tb} \approx 1$, $Z_{wb} \approx 2$ and $Z_f \approx 1$, yielding a ratio of bound electron to free electron scattering of only 3 to 1. This alleviates the spectral contrast required of both the probe source and detection system. It is also instructive to consider the relative importance of undesirable scattering from inevitable shields and mounts. The tightly bound electron scattering contribution / unit area will be ~ Z_{tb}^2mfp, hence ~ $Z^{-1.5}$ since the mfp from above scales as $Z^{-3.5}$. For weakly bound electrons, the Compton scattering contribution will be even less, ~ Z_{wb}mfp ~ $Z^{-2.5}$. Hence, for the reasonable assumption of equivalent areas exposed to the probe photons, scattering from mid Z shields (Z = 20-25) can be kept negligible compared to scattering from Be.

A 0.5-mm-diameter by x = 0.5-mm-long Be cylinder has been chosen as the optimum sample, heated by 4-5 keV pump photons with a 1 mm mfp in cold Be. A laser pulse length of 1 ns extracts maximum power (20 TW) and energy (E = 20 kJ) from 42 Omega beams while restricting the fraction of sample compression and disassembly (disassembly rate ≈ 20 μm/ns at a few eV plasma temperature). One can restrict viewing of the shock front region penetrating at a calculated 50 μm/ns by aperturing or slightly distancing the pump source from the Be sample. The pump laser intensity is then at an optimum $2x10^{15}$ W/cm^2 for efficient production of 4-5 keV x-rays. A CsI conversion layer is chosen as pump source, which has been shown to have 1.5% conversion efficiency to 4-5 keV L-shell x-rays at this laser intensity.[62] The energy absorbed / Be atom at maximum pump power is calculated to be 20 eV, which should provide the few eV solid density plasma temperatures of interest. Higher temperatures can be achieved by doping a smaller Be sample with a more absorptive element, at the expense of reducing the number of potential scatterers. We note that the independence of pump and probe beams allows for varying the sample temperature while keeping the number of probe photons fixed. The energy deposited in the Be sample would be measured on separate shots by using a calibrated crystal spectrometer viewing the transmitted x-rays from planar CsI targets with and without Be overcoats. The combination of electron temperature, density, ionization state and energy absorbed would allow us to answer the important question; how is energy partitioned after equilibriation in low temperature dense plasmas?

The scattering photon energy has then been chosen such that it is not coincident with major n=3 - n=2 transitions of the pump source, and such that its mfp relative to twice the sample size is > 1, yet not so high that its production efficiency is poor. A likely candidate is the He-like V resonance line at 5.2 keV, with a 1.4 mm mfp in Be. Overplotted on Fig. 1 is the predicted electron density of solid Be starting in the metallic state with 1 conduction electron/atom and then progressively ionized[22] above a few eV. The 5.2 keV (2.4 Å) large angle scattering experiment is clearly well suited to this solid density Be regime, with the scattering parameter α increasing from 0.25 to 1 as T_e is reduced from 30 to 1 eV.

The probe solid angle subtended at the sample has been maximized while still allowing for passage of the scattered photons, and shielding of the spectrometer from the probe source (see Fig. 4). In addition, the probe can be considered non-invasive relative to the pump source, having 1/3rd the laser energy (E_T = 6 kJ), 1/5th the x-ray conversion efficiency and 1/10th the solid angle as seen by the Be sample, hence < 1% of the pump strength. When probing the transverse coherence length of the plasma, the probe source coherence can be improved by diminishing the source size with a modest (≈ 3x) loss in number of probe photons. For example, simple optics suggest a 300 μm incoherent probe source size at 1.5 mm from the sample would be able to probe transverse coherence lengths ≈ (1.5/0.3)λ = 12 Å, corresponding to 5-10 interparticle separations at solid density.

A near backscattering geometry (θ = 160°) has been chosen for several reasons. First, blurring of the magnitude of the scattering vector k_s due to a finite range of scattering angles dθ in the experiment can be minimized by operating close to the backscatter direction, since $k_s \approx 2k\sin(\theta/2)$, and hence $dk_s/k_s = d\theta/(2\tan(\theta/2))$ approaches 0 as θ approaches 180°. In the current experimental geometry θ and dθ are set by the desire to minimize the probe stand-off distance and keep θ close to 180°, while simultaneously accomodating for realistic spot sizes and probe laser intensities (≈ 10^{15} W/cm^2). This has led to θ = 160°, dθ = ±15°, and hence an acceptable blurring level of dk_s/k_s = 2%. Second, the scattering efficiency for unpolarized light is 2x greater near 180° than it is for the more traditional 90° geometry. Third, the scattering k vector is maximized as 180° is approached, allowing us to access the incoherent scattering regime ($\alpha = 1/k_s\lambda_D < 1$) and/or shorter wavelength correlations without having to resort to even shorter wavelength probes or having to increase the Debye length by further heating the plasma. Fourth, the advantageous downshift in photon energy hν due to Compton scattering of the photons from both weakly bound electrons and free electrons of mass m_e is greatest at θ = 180°, as given by $d\text{h}\nu/\text{h}\nu \approx -(\text{h}\nu/m_ec^2)(1 - \cos\theta)$ ≈ 0.02 for hν ≈ 5 keV.

The usual Thomson scattering electron feature will be centered around this downshifted incoherent Compton scattering peak. We note that the approximate Doppler broadened halfwidth of the backscattered electron feature for electrons of velocity v is

$\approx 2(\sqrt{2})v/c$ for scattering parameter $\alpha < 1$, which is less than the Compton downshift for plasma temperatures below 30 eV. Hence, by viewing at large scattering angles, we provide a natural spectral isolation from any residual background from the coherent non-spectrally-shifted Rayleigh-type scattering from higher Z shields and mounts surrounding the experiment. The spectral blurring $\delta h\nu/h\nu$ due to the finite range of scattering angles $d\theta$ for Compton scattering is also acceptably small, as given by $\delta h\nu/h\nu = (h\nu/m_ec^2)\sin\theta d\theta$, ≈ 0.001 for $h\nu = 5$ keV, $\theta = 160°$and $d\theta = \pm 15°$.

In addition to the spectral isolation, we envisage delaying the probe by 1 ns and detecting the spectrally dispersed scattered photons by a standard microchannel-plate-based (MCP) framing camera to provide temporal isolation from the background of pump photons. The product of MCP efficiency and filter transmission required to protect the spectrometer and detector is estimated at $\eta_d = 1\%$. Should pump background prove to be minimal, then a 10x more efficient x-ray CCD could replace the MCP detector. At the downshifted energy of 5.1 keV, the diffraction from the efficient LiF 220 Bragg crystal planes (2d spacing = 2.8 Å, integrated reflectivity $R = 10^{-4}$ radians) is available at a moderately dispersive 57° Bragg angle. The angle between spectrometer and detector which is twice the complement of the Bragg angle (66°) can be easily accomodated at Omega by using separate diagnostic ports. By using the crystal in the Von Hamos cylindrically focussing geometry[63] at 8-10 cm (where previous crystals have been successfully fielded undamaged at Nova at similar laser energy), one can further increase the collection solid angle. The maximum reasonable collection angle in the non-dispersive direction as set by the opening aperture defined by the probe foil annulus is large, $\Omega_x \approx 0.3$ radians. The dispersion at the detector can be set such that the source broadening of 0.5 mm translates to a spectral broadening of only $\Delta\lambda/\lambda = 0.001$, small compared to the minimum probe line-width (0.002) and the widths of the Thomson scattered electron features (0.03). A typical 3-cm-long MCP active region will hence accommodate a total spectral coverage $d\lambda/\lambda$ of 0.06, allowing both the V He-like and H-like resonance lines to be detected simultaneously. The unbroadened, unshifted probe spectrum conveniently obtained simultaneously from the coherent scattering component would be deconvolved from the Thomson scattered data.

The expected signal can now be estimated. The number of detected photons N in the electron feature is given by: $N = (E_T\eta_T/h\nu)(\Omega_T/4\pi)(n_e\sigma x/(\alpha^2+1))(\Omega_xR/4\pi)\eta_d$. Recalling that $E_T = 6$ kJ, $\eta_T = .003$, $h\nu = 5$ keV, $\Omega_T/4\pi = 0.01$, $n_e\sigma x/(\alpha^2+1) = 0.002$-$0.003$, $\Omega_xR/4\pi = 2.5\text{x}10^{-5}$, and $\eta_d = 0.01$ leads to N = 10,000 – 15,000 detected photons in the Thomson scattered spectrum. Distributed over say 10 spectral bins, the expected signal-to-noise (SNR) ratio due to photon statistics is excellent, 30-40. It is instructive to consider how the signal scales with usable laser facility energy E and partitioning of pump and probe laser energy. For a given desired sample temperature, the number of heated sample atoms ~ fE, where f is fraction of laser energy used for the pump plasma. Hence, the linear size of the optimized experiment scales as $(fE)^{1/3}$. The number of probe photons reaching the a given sample atom in a scaled experiment is then ~ $\{(1-f)E\}/(fE)^{2/3}$. The signal for fixed detector solid angle varies as the product of the number of potential scatterers and number of probe photons, ~ $(1-f)f^{1/3}E^{4/3}$, yielding a broad optimum around f = 0.25, with only a 2x drop in signal at the current f = 0.75 design point. More interesting is the $E^{4/3}$ scaling, which explains why a smaller laser facility such as Janus, Trident or Vulcan with 1-10 % of the Omega energy would be insufficient, even if 4π laser illumination required for uniform heating were available.

5. SUMMARY

We have designed an x-ray Thomson scattering experiment fully optimized for the Omega laser facility capabilities which should provide high quality spectral data on a single shot. We expect a successful attempt at extending the full versatility of laser Thomson scattering to the x-ray regime to open the door for detailed dense plasma studies of great interest to the high energy density and plasma physics communities.

6. ACKNOWLEDGMENTS

Work performed under the auspices of the U.S. Department of Energy by the University of California Lawrence Livermore National Laboratory under contract number W-7405-ENG-48.

7. REFERENCES

1. J. P. Hansen and I. R. McDonald, "Thermal relaxation in a strongly coupled two-temperature plasma," Phys. Lett. A 97A (1-2), 42-4 (1983).
2. D. B. Boercker, R. W. Lee, and F. J. Rogers, "Strong coupling effects on plasma lineshapes and Thomson scattering signals," J. of Phys. B 16 (17), 3279-90 (1983).
3. S. Ichimaru and S. Tanaka, "Theory of interparticle correlations in dense, high-temperature plasmas. V. Electric and thermal conductivities," Phys. Rev. A 32 (3), 1790-8 (1985).
4. D.B. Boercker and R.M. More, Phys. Rev. A 33, 1859 (1986).

5. J. Meyer-ter-Vehn, A. Oparin, and T. Aoki, "Options for laser compression of matter to study dense-plasma phases at low entropy, including metallization of hydrogen," in 12th International Conference on Laser Interaction and Related Plasma Phenomena, edited by G. Miley and S. Nakai (AIP, Woodbury NY, 1996), Vol. 369, pp. 347-56.
6. A. Ng, A. Forsman, and G. Chiu, "Electron thermal conduction waves in a two-temperature, dense plasma," Phys. Rev. Lett. 81 (14), 2914-17 (1998).
7. A. Forsman, S. Ng, G. Chiu et al., "Interaction of femtosecond laser pulses with ultrathin foils," Phys. Rev. E 58 (2), R1248-51 (1998).
8. S. J. Davidson, K. Nazir, S. J. Rose et al., "Short-pulse laser opacity measurements," J. Quant. Spectrosc. Radiat. Trans. 65 (1-3), 151-60 (2000).
9. D. F. Price, R. M. More, R. S. Walling et al., "Absorption of ultrashort laser pulses by solid targets heated rapidly to temperatures 1-1000 eV," Phys. Rev. Lett. 75 (2), 252-5 (1995).
10. S. M. Cameron, M. D. Tracy, K. G. Estabrook et al., "Two-dimensional electron density, temperature, and radial drift profiles of a laser plasma by 266 nm collective Thomson scattering," Rev. Sci. Instrum. 63 (11), 5259-65 (1992).
11. S. H. Glenzer, W. Rozmus, J. MacGowan et al., "Thomson scattering from high-Z laser-produced plasmas," Phys. Rev. Lett. 82 (1), 97-100 (1999).
12. D. S. Montgomery, R. P. Johnson, J. A. Cobble et al., "Characterization of plasma and laser conditions for single hot spot experiments," Laser Part. Beams 17 (3), 349-59 (1999).
13. Y. Setsuhara, H. Azechi, N. Miyanaga et al., "Secondary nuclear fusion reactions as evidence of electron degeneracy in highly compressed fusion fuel," Laser Part. Beams 8, 609-20 (1990).
14. J. Lindl, "Development of the indirect-drive approach to inertial confinement fusion and the target physics basis for ignition and gain," Phys. Plasmas 2 (11), 3933-4024 (1995).
15. O. Peyrusse, M. Busquet, J. C. Kieffer et al., "Generation of hot solid-density plasmas by laser radiation pressure confinement," Phys. Rev. Lett. 75 (21), 3862-5 (1995).
16. N. C. Woolsey, A. Asfaw, K. B. Hammel et al., "Spectroscopy of compressed high energy density matter," Phys. Rev. E 53 (6), 6396-402 (1996).
17. M. Nantel, G. Ma, S. Gu et al., "Pressure ionization and line merging in strongly coupled plasmas produced by 100-fs laser pulses," Phys. Rev. Lett. 80 (20), 4442-5 (1998).
18. W. Theobald, R. Hassner, R. Kingham et al., "Electron densities, temperatures, and the dielectric function of femtosecond-laser-produced plasmas," Phys. Rev. E 59 (3, pt.A-B), 3544-53 (1999).
19. S. Ichimaru, Rev. Mod. Phys 54, 1017 (1982).
20. H.M. van Horn, The Equation of State in Astrophysics (Cambridge University Press, 1994).
21. S. J. Rose, "The effect of degeneracy on the scattering contribution to the radiative opacity," Astrophys. J. Lett. 453 (1), L45-7 (1995).
22. O. Peyrusse, "A method for calculating the effect of ionization on Thomson scattering," J. Quant. Spectrosc. Radiat. Trans. 43 (5), 397-405 (1990).
23. E. J. Linnebur and J. J. Duderstadt, "Theory of light scattering from dense plasmas," Phys. Fluids 16 (5), 665-74 (1973).
24. O. Theimer and Y. K. Behl, "Electron density fluctuations in a plasma with collision frequency proportional to speed," Plasma Phys. 19 (12), 1119-28 (1977).
25. R. Cauble and D. B. Boercker, "Dynamic structure factors in two-component plasmas," Phys. Rev. A 28 (2), 944-51 (1983).
26. A. W. DeSilva and H. J. Kunze, "Experimental study of the electrical conductivity of strongly coupled copper plasmas," Phys. Rev. E 49 (5), 4448-54 (1994).
27. I. Krisch and H. J. Kunze, "Measurements of electrical conductivity and the mean ionization state of nonideal aluminum plasmas," Phys. Rev. E 58 (5), 6557-64 (1998).
28. A. W. DeSilva and J. D. Katsouros, "Electrical conductivity of dense copper and aluminum plasmas," Phys. Rev. E 57 (5), 5945-51 (1998).
29. J. F. Benage, Jr., W. R. Shanahan, E. G. Sherwood et al., "Measurement of the electrical resistivity of a dense strongly coupled plasma," Phys. Rev. E 49 (5), 4391-6 (1994).
30. W. Rozmus and A. A. Offenberger, "Thermal conductivity for dense, laser-compressed plasmas," Phys. Rev. A 31 (2), 1177-9 (1985).
31. A. N. Mostovych, K. J. Kearney, J. A. Stamper et al., "Measurements of plasma opacity from laser-produced optically thin strongly coupled plasmas," Phys. Rev. Lett. 66 (5), 612-15 (1991).
32. K. Eidmann, A. Bar-Shalom, A. Saemann et al., "Measurement of the extreme UV opacity of a hot dense gold plasma," Europhys. Lett. 44 (4), 459-64 (1998).
33. P. Gauthier, S. J. Rose, P. Sauvan et al., "Modeling the radiative properties of dense plasmas," Phys. Rev. E 58 (1), 942-50 (1998).

34. D. Liberman and J. Albritton, "Dense plasma equation of state model," J. Quant. Spectrosc. Radiat. Trans. 51 (1-2), 197-200 (1994).
35. F. Perrot and M. W. C. Dharma-Wardana, "Equation of state and transport properties of an interacting multispecies plasma: application to a multiply ionized Al plasma," Phys. Rev. E 52 (5), 5352-67 (1995).
36. O. L. Landen and R. J. Winfield, "Laser scattering from dense cesium plasmas," Phys. Rev. Lett. 54 (15), 1660-3 (1985).
37. G. R. Bennett, J. S. Wark, D. J. Heading et al., "Production of strongly coupled plasmas by the laser irradiation of thin metallic films confined within micrometer-scale gaps by transparent insulators," Phys. Rev. E 50 (5), 3935-42 (1994).
38. A. N. Mostovych and Chan Yung, "Reflective probing of the electrical conductivity of hot aluminum in the solid, liquid, and plasma phases," Phys. Rev. Lett. 79 (25), 5094-7 (1997).
39. H. M. Milchberg, R. R. Freeman, and S. C. Davey, "Resistivity of a simple metal from room temperature to 10/sup 6/ K," Phys. Rev. Lett. 61 (20), 2364-7 (1988).
40. A. Ng, P. Celliers, A. Forsman et al., "Reflectivity of intense femtosecond laser pulses from a simple metal," Phys. Rev. Lett.72 (21), 3351-4 (1994).
41. M. H. Mahdieh and T. A. Hall, "Optical reflectivity of dense plasmas produced by laser driven shock waves," J. of Phys. D 30 (4), 588-92 (1997).
42. C. Quoix, G. Hamoniaux, A. Antonetti et al., "Ultrafast plasma studies by phase and amplitude measurements with femtosecond spectral interferometry," J. Quant. Spectrosc. Radiat. Trans. 65 (1-3), 455-62 (2000).
43. O. L. Landen, D. G. Stearns, and E. M. Campbell, "Measurement of the expansion of picosecond laser-produced plasmas using resonance absorption profile spectroscopy," Phys. Rev. Lett. 63 (14), 1475-8 (1989).
44. O. L. Landen and W. E. Alley, "Dynamics of picosecond-laser-pulse plasmas determined from the spectral shifts of reflected probe pulses," Phys. Rev. A 46 (8), 5089-100 (1992).
45. D. K. Bradley, J. Kilkenny, S. J. Rose et al., "Time-resolved continuum-edge-shift measurements in laser-shocked solids," Phys. Rev. Lett. 59 (26), 2995-8 (1987).
46. T. A. Hall, A. Djaoui, R. W. Eason et al., "Experimental observation of ion correlation in a dense laser-produced plasma," Phys. Rev. Lett. 60 (20), 2034-7 (1988).
47. D. Riley, O. Willi, S. J. Rose et al., "Blue shift of the K absorption edge in laser-shocked solids," Europhys. Lett. 10 (2), 135-40 (1989).
48. D. J. Heading, G. R. Bennett, J. S. Wark et al., "Novel plasma source for dense plasma effects," Phys. Rev. Lett. 74 (18), 3616-19 (1995).
49. B. A. Shiwai, A. Djaoui, T. A. Hall et al., "Improvements to ion-correlation experiments in dense plasmas," Laser Part. Beams 10 (1), 41-51 (1992).
50. E. A. Oks, S. Boddeker, and H. J. Kunze, "Spectroscopy of atomic hydrogen in dense plasmas in the presence of dynamic fields: Intra-Stark spectroscopy," Physical Review A 44 (12), 8338-47 (1991).
51. N. C. Woolsey, D. Riley, and E. Nardi, "Kilovolt x-ray scattering from a plasma," Rev. Sci. Instrum. 69 (2 PT1), 418-424 (1998).
52. E. Nardi, Z. Zinamon, D. Riley et al., "X-ray scattering as a dense plasma diagnostic," Phys. Rev. E 57 (4), 4693-4697 (1998).
53. D. Riley, N. C. Woolsey, D. McSherry et al., "X-ray scattering from a radiatively heated plasma," J. Quant. Spectrosc. Radiat. Trans. 65 (1-3), 463-470 (2000).
54. N. B. McNelis and A. W. DeSilva, "Experimental tests of light scattering theory in plasmas," Plasma Phys. 24 (10), 1261-75 (1982).
55. J.H. Hubbell, W.J. Weigele, E.A. Briggs et. al., "Atomic form factors, incoherent scattering functions, and photon scattering cross sections," J. Phys. Chem. Ref. Data 4, 471-533 (1975).
56. W.J. Weigele, P.T. Tracy, and E.M. Henry, "Compton effect and electron binding," Am. J. Phys. 34, 1116-1121 (1966).
57. P.A. Ross and P. Kirkpatrick, "Effect of electron binding upon the magnitude of the Compton shift," Phys. Rev. 46, 668-673 (1934).
58. F. Bloch, "Contribution to the theory of the Compton-line," Phys. Rev. 46, 674-687 (1934).
59. D.A. Liberman, Phys. Rev. B 20, 4981 (1979).
60. D.E. Kelleher, private communication (1999).
61. S. G. Glendinning, P. Amendt, K. S. Budil et al., "Laser plasma diagnostics of dense plasmas," in Applications of Laser Plasma Radiation II, edited by G. Kyrala (SPIE, Bellingham, 1995), Vol. 2549, pp. 29-39.
62. C. A. Back, J. Grun, C. Decker, L. J. Suter et. al., "Efficient multi-keV underdense laser-produced plasma radiators," submitted to Phys. Rev. Lett. (2000).
63. B. Yaakobi, R. E. Turner, H. W. Schnopper et al., "Focusing X-ray spectrograph for laser fusion experiments," Rev. Sci. Instrum. 50 (12), 1609-11 (1979).